Heliyon 10 (2024) e33709

Contents lists available at ScienceDirect

Heliyon

journal homepage: www.cell.com/heliyon

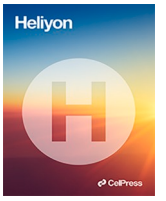

Research article

Tuning optical, magnetic, and electrical parameters of $CuFe_2O_4$ nanoparticles incorporated with GO and ZnO using a facile synthesis

Saddam Hussain [a], Samavia Rafiq [a], M.I. Yousaf [a,*], Sofia Nosheen [b], Dalal Nasser Binjawhar [c], Mohamed M. Abdel-Daim [d,e]

[a] Department of Applied Sciences, National Textile University, Faisalabad, Pakistan
[b] Department of Environmental Sciences, Lahore College For Women University, Lahore, Pakistan
[c] Department of Chemistry, College of Science, Princess Nourah bint Abdulrahman University, P.O. Box 84428, Riyadh, 11671, Saudi Arabia
[d] Department of Pharmaceutical Sciences, Pharmacy Program, Batterjee Medical College, P.O. Box 6231 Jeddah 21442, Saudi Arabia
[e] Pharmacology Department, Faculty of Veterinary Medicine, Suez Canal University, Ismailia, 41522, Egypt

ARTICLE INFO

Keywords:
Facile synthesis
$CuFe_2O_4$/GO/ZnO
Magnetic properties
Optical properties
Electrical properties

ABSTRACT

Nano-ferrites, metal oxides, and carbon-based nanomaterials have been used frequently to enhance optical and magnetic prospects for latent applications. Copper ferrite/Graphene Oxide and Zinc Oxide ($CuFe_2O_4$/GO/ZnO) ternary nanocomposite synthesized by hydrothermal route showed dramatically good outcomes as the band gap energy value of synthesized nanocomposite approaches to 2.4 eV. Furthermore, the light absorbance of $CuFe_2O_4$ increases by adding ZnO and GO. The experimental data revealed the face-centered cubic structure (FCC) of pure spinal ferrite ($CuFe_2O_4$) nanoparticles even after adding ZnO and GO. The 2θ peak observed at 31.70° with (220) hkl planes indicates the successful addition of ZnO nanoparticles in $CuFe_2O_4$/GO nanocomposite. XRD graph, the absence of characteristic peaks of GO revealed the intercalation of $CuFe_2O_4$ nanoparticles with GO layers. In SEM images, agglomeration among $CuFe_2O_4$ nanoparticles is observed due to the magnetic interaction of nano-crystallite with a high surface-to-volume (S/V) ratio. VSM can be used to determine the magnetic properties of as-synthesized samples at moderate temperatures under 0–0.5 and ± 5 tesla. In $CuFe_2O_4$/GO/ZnO ternary nanocomposite, the saturation magnetization value reduces from 2.071 to 1.365 emu/g due to the addition of ZnO nanoparticles. The loops were narrowed showing a decrease in the coercive field with the addition of ZnO nanoparticles in $CuFe_2O_4$/GO ternary nanocomposite material. Moreover, the study of electrical properties of pure $CuFe_2O_4$ and $CuFe_2O_4$/GO/ZnO ternary nanocomposite revealed that the values of dielectric constant and tangent loss decrease at high frequencies owing to surface charge polarization and intrinsic dipole interactions. The study of the electrical properties of both pure $CuFe_2O_4$ and the $CuFe_2O_4$/GO/ZnO ternary nanocomposite reveals that the dielectric constant (ε') and tangent loss (tanδ) exhibit a decreasing trend as the frequency increases. This behavior is attributed to surface charge polarization and intrinsic dipole interactions. At lower frequencies, both samples display elevated values for these properties, which stabilize as the frequency increases beyond 2 MHz. Notably, high AC conductivity is observed in both samples, attributed to increased capacitance and resistance.

* Corresponding author.
E-mail addresses: muhammadsaddam888@gmail.com (S. Hussain), imran@ntu.edu.pk (M.I. Yousaf).

https://doi.org/10.1016/j.heliyon.2024.e33709
Received 26 April 2024; Received in revised form 25 June 2024; Accepted 26 June 2024
Available online 27 June 2024

1. Introduction

Nano-ferrites belong to the family of spinel magnetic materials and have been used recently in various applications i.e., magnetic resonance imaging (MRI), sensors, electromagnetic shielding, transformer inductors, and memory core devices owing to their exceptional magnetic as well as dielectric prospects [1]. Heating, cooling time, grinding as well as high temperature tend to increase the physical and chemical properties of nano-ferrites. Even a small addition of any other ions in the nano-ferrites can change their chemical composition drastically. Spinel ferrites are used as magnetic materials in different fields due to their low cost, high resistivity, wide-frequency range, superior magnetic properties, and high sensitivity to visible light [2]. The basic chemical formula of ferrites AB_2O_4 indicates the divalent cations and trivalent metal ions. The spinel structure is formed when the octahedral (A) and tetrahedral (B) sites are occupied by the distribution of cations (e.g., A = Cu^{2+}, Ni^{2+}, Mn^{2+}, $Zn^{2+,}$ and B═Fe^{3+}) [3]. One of the dominant spinel ferrites is Copper ferrite ($CuFe_2O_4$), it displays the stage conversion, and exchange of semi-conducting effects, and reveals variation in the direction of electrical current when surged under individual conditions in inclusion to compel magnetic and optical effects with chemical and thermal stability [4]. $CuFe_2O_4$ is used in a wide range of applications i.e., gas sensing, catalytic, color imaging, bio-purifying, Li-ion batteries high bulk magneto-optic videotape devices, and magnetic freezing. In addition, due to the high electric conductivity and thermal stability, $CuFe_2O_4$ is assumed to be a magnetic and dielectric material of great potential [5,6]. However, easy recombination of electron-hole pair and high agglomeration in the solution are the drawbacks that affect the performance of $CuFe_2O_4$ during various applications. Coupling $CuFe_2O_4$ with porous materials having a large surface area can overcome the drawbacks. For that purpose, among semi-conducting metal oxide materials like ZnO nanoparticles have gained popularity for their high stability and high band gap energy which could easily enhance the oxidizing activity when dispersed together with $CuFe_2O_4$ [7]. ZnO is an excellent semiconductor and it belongs to the II-VI semiconductor family as it has a direct band gap energy of 3.37eV and high excitation binding energy at room temperature [8]. Excellent dielectric properties, sensible transparency, high negatron quality, and wide band gap are the main properties of ZnO. These properties turn ZnO into an asset in applications like solar cells, photocatalysts, heat-preserve windows, thin-film transistors, and light-discharge diodes [9–11], as for the magnetic loss properties which cannot satisfy the strong absorption and broad-band gap requirements of the nanomaterials.

Graphene Oxide (GO) is a two-dimensional carbon material with high mechanical strength, high electrical conductivity, and specific area paramagnetic and biocompatible properties. It also has high optical transmittance in the visible spectrum region. GO has outstanding properties of huge extent and mechanical and thermal stability. GO has implementations in nuclear system cooling, house and safeguarding, star absorption, mechanical application, magnetic protection, medical skill application, heat transfer electronic employment, laser applications, industrial cooling utilization, photocatalysis, and decreasing pollution [12–14]. In response to optical properties, GO suggestively resists the electron-hole pair rejoining rate results to enhance the optical activity or photocatalytic activity of the composite materials. For degradation purposes, if GO is coupled with appropriate UV–visible light semiconductor nano-composites it can lead to efficient photodegradation activity during photocatalysis or optical applications [15]. Not only optically or magnetically but also the study of electrical as well as dielectric behavior is similarly substantial to both fundamental as well as applied viewpoint. In the comparison of GO binary nanocomposite complexes with the others, recently the GO ternary nanocomposite complexes show greater potential for enhancing the optical and electrical prospects of nanocomposite samples. So, the combination of magnetic nano-ferrite $CuFe_2O_4$, semiconductive metal oxide ZnO, and non-magnetic GO can show synergistic effects not only at the same time but also can be beneficial in optical, electrical, and magnetic parameters. So, the combination of nano-ferrite/carbon material/metal oxide demonstrates high electrochemical behavior owing to redox reaction, large surface-to-volume ratio(S/V), and excellent conductivity.

Some convenient techniques for preparing the nano-ferrites include a hydrothermal method, sol-gel process, microwave combustion, wet chemical, and co-precipitation methods. The hydrothermal route is attractive because it can offer homogenous (dispersed) samples with good crystallinity, mild operating conditions (i.e., low temperature $<300\ ^{\circ}C$), high yield and purity, and eco-friendly and one-step procedure.

The present study aims to decrease the energy band gap of pure $CuFe_2O_4$nanodots by adding GO nanosheets and ZnO nanoparticles to enhance their optical properties. Additionally, for improving the magnetic and electrical properties of pure $CuFe_2O_4$ nanoparticles, ZnO nanoparticles act as a boosting material– they exhibit intrinsic ferromagnetic behavior and have extraordinary dielectric properties. The hydrothermal route carries out the synthesis of $CuFe_2O_4$/GO/ZnO ternary nanocomposite and undergoes different characterization techniques to determine structural and spectroscopic parameters of the ternary nanocomposite. Moreover, analyzing optical, magnetic, as well as electrical prospects of the $CuFe_2O_4$/GO/ZnO ternary nanocomposite which could be further utilized as a potential candidate for various applications e.g., as a catalyst, light emitting diodes, water treatment, magnetic storage, fuel cells, sensors, etc.

2. Experimental section

2.1. Materials

Iron nitrate ($Fe(NO_3)_3{\cdot}9H_2O$), Copper nitrate ($Cu(NO_3)_2\ 3H_2O$), as well as Zinc oxide nanoparticles (ZnO) were purchased out of Sigma-Aldrich, USA. Sanitized water and deionized water were used as a solvent and were prepared in the lab. All materials were analyzed as reagents and used as received without further purification.

Graphite powder (99.99 % purity) was bought from Merck & Co. Chemicals, New Jersey, USA. Using Hummer's method, graphene oxide (GO) was synthesized by graphite powder.1.5 g of graphite powder with 3 g of $NaNO_3$ and both of them were dispersed in the H_2SO_4 ice bath. A specific amount of $KMnO_4$ was added under vigorous stirring. The dispersion was sonicated for 30 min, kept at 90 °C for 24 h, and further treated with deionized water and H_2O_2. Deionized water was used to wash the GO nanosheets many times till their pH reached 7 and at the end, a vacuum oven was used to dry the as-synthesized nanosheets at 65 °C for 24 h.

2.1.1. Synthesis of $CuFe_2O_4$/GO/ZnO ternary nanocomposite

As for copper ferrite ($CuFe_2O_4$), 100 ml distilled water is added in 1.5 g and 4 g of metal salt precursors iron nitrate ($Fe(NO_3)_3{\cdot}9H_2O$) and copper nitrate ($Cu(NO_3)_2{\cdot}3H_2O$) to form an aqueous solution. The pH of this aqueous solution is maintained by the use of NaOH. The aqueous dispersion was sonicated and stirred for 45 min. Then, the dispersion was put into an autoclave vessel at 130 °C for 1 h. The solution was washed several times with sanitized water and centrifuged5 times at 3000 rpm for 30 min. At 200 °C sintering temperature for 24 h, the solvent evaporated, and the final product was obtained.

For the synthesis of $CuFe_2O_4$/GO/ZnO ternary nanocomposite, 0.06 g GO was added into 50 ml distilled water to prepare a dispersion. In another beaker, 0.5 g ZnO nanoparticles were added in 50 ml distilled water to form another dispersion. 1.5 g prepared sample of $CuFe_2O_4$ mixed in 100 ml distilled water. All dispersions were sonicated for 35 min separately and then added together in a single beaker. The solution was sonicated again for 15 min to obtain uniform dispersion. The solution was poured into the autoclave vessel and put into the autoclave chamber overnight at 110 °C. After the mixture precipitates overnight, it filters again and again till the pH adjusts to 7. The product was dried at room temperature and then put in a vacuum oven at 60 °C overnight. The $CuFe_2O_4$/GO/ZnO ternary nanocomposite was grinding into a fine powder for characterization purposes. The design of the experiment is shown in Table 1.

2.2. Analytical characterization

For X-ray diffraction(XRD), an X-ray diffractometer (XRD, X'Pert XRD) having a radiation source of CuKα (1.54 Å) functioned in the 2θ range of 10–80° determines the crystalline and phase properties of the as-synthesize sample. Scanning electron microscopy (SEM) – (FEI Quanta 250, USA) attached with energy dispersive X-ray (EDX) determines the surface morphology and elemental composition of the as-synthesized sample and transmission electron detectors operated at an accelerating voltage of 15 kV. Fourier transform infrared spectroscopy (FTIR)was used to analyze the chemical bonding amongst the materials recorded on a (ATR-FTIR) Bruker Tensor 27 spectroscope in the wavenumber range of 4000-600 cm^{-1}. The optical spectra and parameters of the prepared ternary nanocomposite were analyzed using a UV–Vis spectrophotometer (UV-1800, Shimadzu, Japan) having a resolution of 1 nm and a wavelength range of 200–1100 nm. A vibrating sample magnetometer (VSM, DXV-9000 series, Xiamen Dexing Magnet Tech Co., Ltd) can be used to determine the magnetic parameters of the prepared sample having a maximum magnetic field of 10 mOe. The electrical properties i.e., dielectric constant, dielectric loss, tangent loss, and AC conductivity were analyzed by Frequency Response Analyzer (Impedance/Gain-phase analyzer) using model Solartron 1260 in the frequency range of 20 mHz–2 MHz at room temperature.

3. Results & discussion

3.1. XRD analysis

The structure composition and crystallite size of pure $CuFe_2O_4$, $CuFe_2O_4$/GO, and $CuFe_2O_4$/GO/ZnO were investigated by XRD graphs as shown in Fig. 1. Diffraction peaks of $CuFe_2O_4$observed at 2θ (35.64°, 43.04°) corresponding to hkl values (400), (511) respectively [16]. The experimental data revealed the face cubic structure of pure spinal ferrite ($CuFe_2O_4$) nanoparticles. Moreover, no additional impurity peaks (CuO or Cu_2O) were observed in the spectrum of raw $CuFe_2O_4$ nanoparticles. The diffraction peaks of $CuFe_2O_4$/GO nanocomposite at 2θ (33.36°,53.37°,75.48°), all corresponded to the crystal planes hkl (311), (511), (215) of $CuFe_2O_4$ nanoparticles (JCPDS card no: 85–1326). As shown in Fig. 1, the diffraction pattern of $CuFe_2O_4$ was like $CuFe_2O_4$/GO nanocomposite. As no peak of GO seemed in the spectrum of the nanocomposite suggested that $CuFe_2O_4$/GO nanocomposite was fully exfoliated owing to the crystal growth of $CuFe_2O_4$ nanodots among the interlayers of GO which caused small diffraction intensity of GO [17]. The diffraction peaks of prepared $CuFe_2O_4$/GO/ZnO ternary nanocomposite observed at 2θ (31.70°, 33.36°, 36.85°, 41.54°, 53.37°, 63.04°, 66.84°, 75.48°) consistent to hkl values (220, 311, 331, 400, 511, 440, 112, 215) respectively. The peaks of $CuFe_2O_4$ and $CuFe_2O_4$/GO were well-matched with the literature [18,19]. As mentioned above, even with the addition of ZnO nanoparticles – the face structure of $CuFe_2O_4$/GO/ZnO ternary nanocomposite is cubic. The presence of a peak at 2θ(31.70°) with an hkl value (220)

Table 1
Design of Experiment of Cu $CuFe_2O_4$/GO/ZnO ternary nanocomposite.

Precursor	$CuFe_2O_4$ nanoparticles	$CuFe_2O_4$/GO nanocomposite	$CuFe_2O_4$/GO/ZnO ternary nanocomposite
$(Fe(NO_3)_3\ 9H_2O)$	1.5 g	–	–
$(Cu(NO_3)_2\ 3H_2O)$	4 g	–	–
$CuFe_2O_4$	–	1.5 g	1.5 g
GO	–	0.06 g	0.06 g
ZnO	–		0.5 g

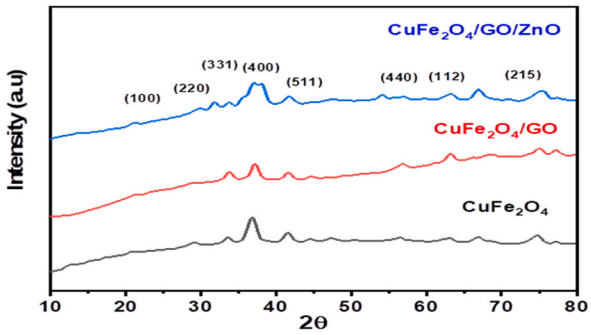

Fig. 1. X-ray diffraction pattern of pure $CuFe_2O_4$ nanoparticles, $CuFe_2O_4$/GO nanocomposite, and $CuFe_2O_4$/GO/ZnO ternary nanocomposite.

indicates the successful addition of ZnO in $CuFe_2O_4$/GOnanocomposite. The doubling of diffraction peaks appears to be an accumulation of ZnO peak with $CuFe_2O_4$ nanoparticles peak and claims the formation of nano-size particles whereas the crystal size of the $CuFe_2O_4$ is ~51.23 nm, while the crystal size of $CuFe_2O_4$/GO/ZnO ternary nanocomposite is ~57.54 nm calculated by using the Debye-Scherrer formula.

While the manuscript indicates a higher ZnO content in the composite, the actual ZnO amount may be insufficient to yield distinct peaks in the XRD pattern. Potential reasons for this include the synthesis method or the ZnO concentration in the final product. The XRD pattern of the $CuFe_2O_4$/GO/ZnO ternary nanocomposite exhibits peaks at 2θ values of 31.70° and 57.54 nm, attributed to $CuFe_2O_4$ and ZnO presence. However, these peaks may overlap, hindering the differentiation of individual ZnO peaks. The similarity in lattice parameters between $CuFe_2O_4$ and ZnO could contribute to this overlap. Furthermore, ZnO peaks perfectly concede with the following linked literature [20]. Additionally, the crystal size and morphology of the $CuFe_2O_4$/GO/ZnO nanocomposite may impact the clarity and sharpness of XRD peaks.

3.2. SEM analysis

The topographical morphology of as-synthesized $CuFe_2O_4$, $CuFe_2O_4$/GO nanocomposite, and $CuFe_2O_4$/GO/ZnO ternary nanocomposite are shown in Fig. 2. SEM micrographs of prepared samples revealed amorphous nature and cubic crystal structure as mentioned in XRD analysis. No definitive morphology is noticed. Fig. 2a, b designates that the $CuFe_2O_4$ nanoparticles have crystalline morphology, and compact arrangement and are embedded homogeneously into the GO layers. This indicates the homogenous distribution of $CuFe_2O_4$ nanoparticles may be a reason for enhanced optical parameters which will be discussed later [21]. The shape of the $CuFe_2O_4$ nanoparticles is cubic. The $CuFe_2O_4$/GO/ZnO ternary nanocomposite showed agglomerated spherical morphology in Fig. 2c. This was caused due to the essential magnetic interaction among the nano-crystallites and large surface-to-volume area that caused agglomeration [22].

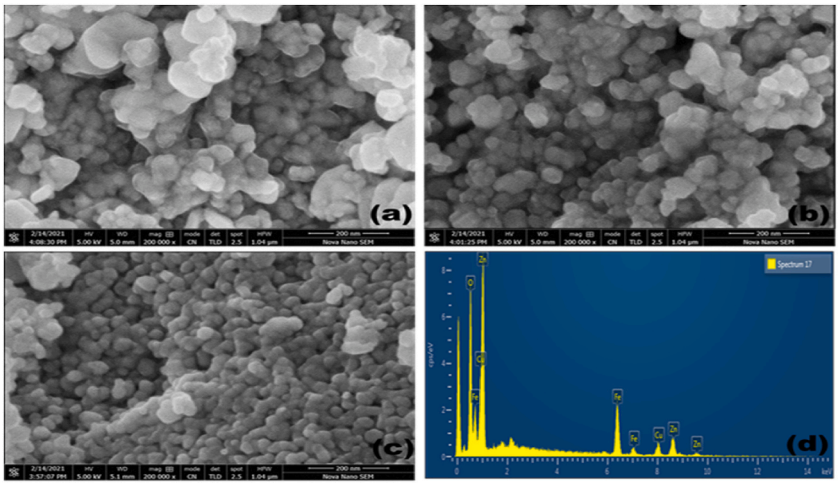

Fig. 2. SEM micrographs of (a) pure $CuFe_2O_4$ nanoparticles(b) $CuFe_2O_4$/GO nanocomposite (c) $CuFe_2O_4$/GO/ZnO ternary nanocomposite (d) EDX spectra $CuFe_2O_4$/GO/ZnO ternary nanocomposite.

3.3. EDX analysis

To define the elemental composition of $CuFe_2O_4$/GO/ZnO ternary nanocomposite, EDX analysis was undertaken. The EDX spectra of the ternary as-synthesized sample are shown in Fig. 2d. According to the spectra, it shows that Cu, Fe, C, O, and Zn elements are distributed all over the surface, indicating the successful formation of the nanocomposite. The$CuFe_2O_4$/GO/ZnO ternary nanocomposite consists of 22.45 % (O), 22.85 % (Fe),13.51 % (Cu), and 41.19 % (Zn) content as shown in Table 2.

3.4. FTIR analysis

The functional group measurement and their chemical bonding in ternary material were done by FTIR analysis. The FTIR spectra of raw $CuFe_2O_4$, $CuFe_2O_4$/GO, and $CuFe_2O_4$/GO/ZnO are shown in Fig. 3. The graph shows a broad absorption peak around 3500 cm^{-1} that resembles the stretching vibrations of water molecules (O–H) group. The depth (intensity) of this peak decreases owing to the evaporation process of H_2O molecules during synthesis [22]. The spectra of pure $CuFe_2O_4$ associated with stretching vibrations of (Fe–O) metal-oxygen group at 750-650 cm^{-1}. The intensity of this peak increases when ZnO (metal-oxide nanoparticles) is added to the $CuFe_2O_4$/GO nanocomposite. The peaks at 1398 cm^{-1}, 1405 cm^{-1}, and 1648 cm-1 are recognized to be symmetrical as well as anti-symmetrical stretching vibrations of COO groups as C═O, C–C, and C–O band vibrations. There are light peaks in pure $CuFe_2O_4$ which may attributed to C ≡C bond which almost diminishes in the $CuFe_2O_4$/GO/ZnO ternary nanocomposite which may be due to high temperature during synthesis [23]. In the case of GO characteristic peaks in $CuFe_2O_4$/GO nanocomposite attributed to 859 cm^{-1} and 1047 cm^{-1}remainepoxy C–O stretching and alkoxy C–O stretching vibrations. The peaks in $CuFe_2O_4$/GO/ZnO ternary nanocomposite originate at 2995 cm^{-1}, 1514 cm^{-1}, and 1392 indicating the presence of C–H, N–H, and O–H groups.

Generally, in spinel ferrites, the two absorption bands can be noticed. In the FTIR spectrum of $CuFe_2O_4$/GO/ZnO ternary nanodots, the peaks appear within the range of 600–700 cm^{-1} attributed to the Fe^{3+}tetrahedral sites whereas the peaks in 600–550 cm^{-1}correspond to Cu^{2+}octahedral sites [24]. So, the peaks in these ranges can be acknowledged as absorption peaks of copper ferrite nanodots.

3.5. UV–visible spectroscopy

The optical properties play a dynamic role in improving the photocatalytic activity of nanoparticles or nanocomposites. UV–Vis absorbance spectra of pure $CuFe_2O_4$, $CuFe_2O_4$/GO nanocomposite and $CuFe_2O_4$/GO/ZnO ternary nanocomposite as shown in Fig. 4. The $CuFe_2O_4$nanoparticles showed absorbance peaks in the region of 350 nm–550nm having a distinct peak at 362 nm as shown in Fig. 4a and a shoulder peak at 390 nm which corresponds to n-π* transition of C═O bonds which is also well matched with the previous literature [25,26]. The $CuFe_2O_4$/GO nanocomposite has shown a similar spectrum but with a broad peak at 380 nm. The absorbance of $CuFe_2O_4$/GO nanocomposite was decreased by adding GO nanosheets compared to pure $CuFe_2O_4$ nanoparticles. Still, the peak of $CuFe_2O_4$/GO nanocomposite was slightly broader as compared to pure $CuFe_2O_4$ nanoparticles as is visibly shown in Fig. 4b.

The absorbance of $CuFe_2O_4$ nanoparticles decreased when we added GO nanosheets within the sample but with the addition of ZnO nanoparticles the absorbance of nanocomposite increased as shown in Fig. 4c, which means that the enhanced absorption peak within the region of 350 nm–400nm shows an increase in the absorbance and decrease in wavelength spectra of $CuFe_2O_4$/GO/ZnO ternary nanocomposite.

Through UV–vis spectra, the band gap energy of as-synthesized $CuFe_2O_4$/GO/ZnO ternary nanocomposite is determined by using Tauc's plot method. According to the obtained data, the band gap energy of pure $CuFe_2O_4$ nanoparticles is 2.63eV. After the addition of GO in pure $CuFe_2O_4$ nanoparticles, the value of the energy band gap becomes 2.51eV. Whereas the value of direct band gap energy of CuFe2O4/GO/ZnO ternary nanocomposite approaches 2.46eV after including the ZnO nanoparticles into the ternary nanocomposite as shown in Fig. 5.

The value of the energy band gap of nanocomposite is decreased related to raw $CuFe_2O_4$ and ZnO nanoparticles. This is owing to the increasing surface defects of various concentrations in energy levels within valence and conduction bands of nanocomposite which facilitates the activation towards visible light. Another reason for the decrease in band gap energy is the superior ionic radius of nanocomposite metals in comparison to base metals leads to increasing disorder in the system. This disorder is more distinct in the lower energy region of the band gap, where the bending of the band occurs due to the interaction of valence bond holes and conduction band electrons [27,28].

Table 2
Elemental composition percentage of Cu $CuFe_2O_4$/GO/ZnO ternary nanocomposite.

Element	Line type	$CuFe_2O_4$/GO/ZnO (wt.%)
C	K series	2
O	K series	21.45
Fe	K series	21.85
Cu	L series	13.51
Zn	L series	41.19

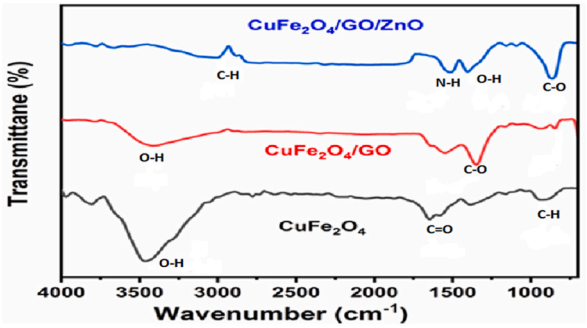

Fig. 3. FTIR pattern of pure $CuFe_2O_4$ nanoparticles, $CuFe_2O_4$/GO nanocomposite, and $CuFe_2O_4$/GO/ZnO ternary nanocomposite.

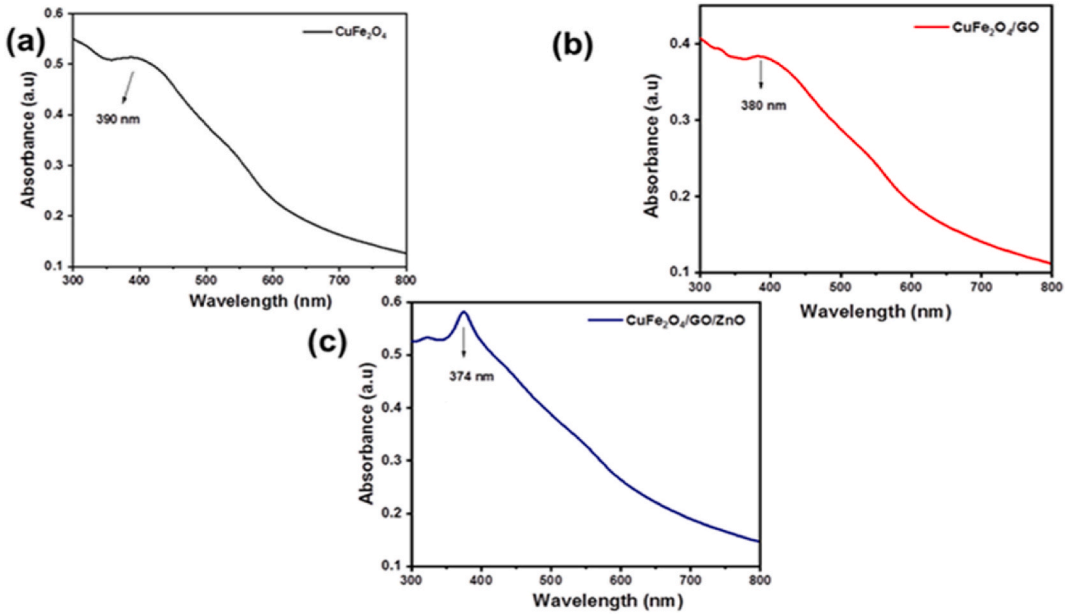

Fig. 4. UV–visible spectra of (a) pure $CuFe_2O_4$ nanoparticles, (b) $CuFe_2O_4$/GO nanocomposite, (c) $CuFe_2O_4$/GO/ZnO ternary nanocomposite.

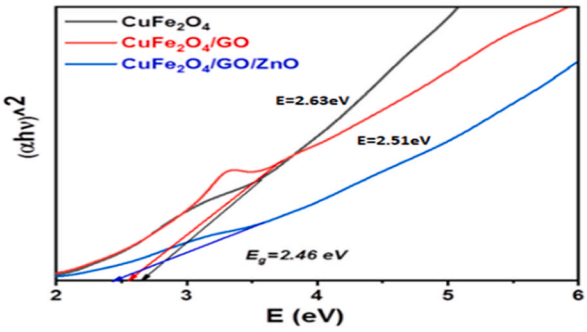

Fig. 5. Band gap energy of pure $CuFe_2O_4$ nanoparticles, $CuFe_2O_4$/GO nanocomposite, $CuFe_2O_4$/GO/ZnO ternary nanocomposite.

3.6. Magnetic analysis

The physical as well as chemical properties of prepared samples may vary from their bulk form, mainly due to nanoscale size. Magnetic materials like $CuFe_2O_4$ act as a huge paramagnetic atom that gives a quick response to a magnetic field when placed or applied to it [29]. The basic magnetic properties i.e., saturation magnetism (M_s), remnant magnetism (M_r) as well as coercivity (H_c) of

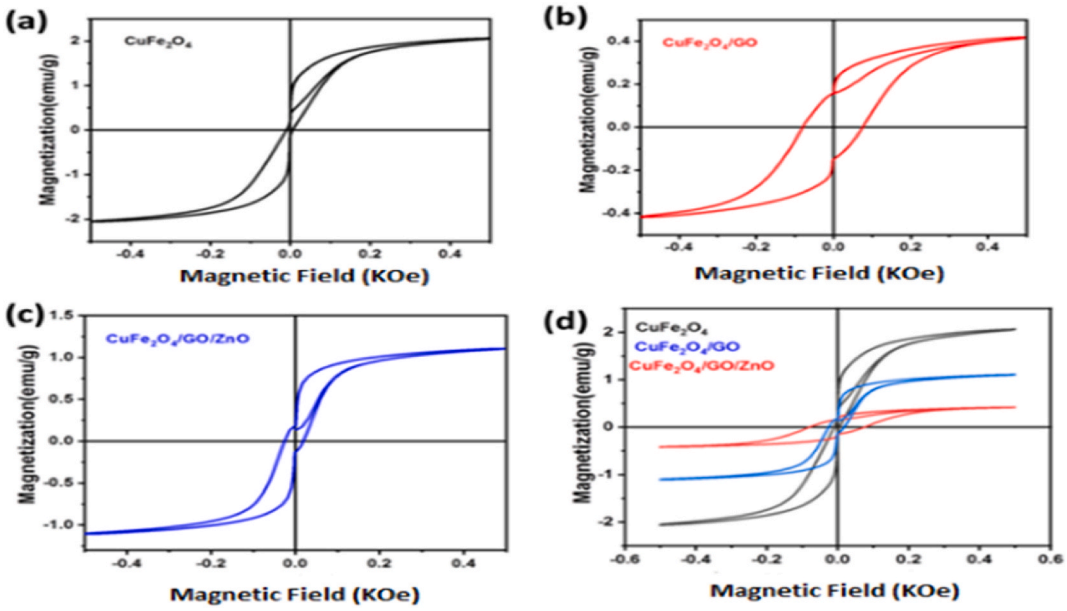

Fig. 6. VSM hysteresis loop of magnetization (a) pure $CuFe_2O_4$ nanoparticles, (b) $CuFe_2O_4$/GO nanocomposite, (c) $CuFe_2O_4$/GO/ZnO ternary nanocomposite, (d) Comparison of pure $CuFe_2O_4$ with $CuFe_2O_4$/GO/ZnO ternary nanocomposite.

pure $CuFe_2O_4$ [Fig. 6a], $CuFe_2O_4$/GO [Fig. 6b] nanocomposite and $CuFe_2O_4$/GO/ZnO [Fig. 6c] ternary nanocomposite were evaluated through a hysteresis loop. The characterization was carried out at room temperature via VSM analysis under 0–0.5 and ± 5 T. Plots of pure$CuFe_2O_4$, $CuFe_2O_4$/GO nanocomposite, and $CuFe_2O_4$/GO/ZnO ternary nanocomposite are shown in Fig. 6. The graph reveals that the hysteresis loop of pure $CuFe_2O_4$ indicates the normal ferromagnetic behavior of magnetic material. For pure$CuFe_2O_4$, Saturation magnetization (M_s), remnant magnetization (M_r), and coercivity (H_c) have the values 2.071emu/g, 0.788emu/g, and 0.00984 kOe. As for the $CuFe_2O_4$/GO nanocomposite, the saturation magnetization (M_s) was 1.992 emu/g which shows the superparamagnetic behavior of nanocomposite. It appears that the saturation magnetization (M_s) reduces after the packing of GO [21]. Moreover, for $CuFe_2O_4$/GO/ZnOternary nanocomposite, the same hysteresis loop of ferrites is identified. The value of saturation magnetization decreases to 1.365 emu/g with the addition of ZnO as shown in Fig. 6c.In ternary nanocomposite, the loops were narrowed showing a decrease in coercive field with the addition of ZnO content in $CuFe_2O_4$/GO nanocomposite material. The decrease in saturation magnetization behavior of nanocomposite can be well explained by the Sawatzky model. Hence, it can result in the hyper-fine field reduced by the addition of ZnO content in $CuFe_2O_4$/GO nanocomposite. It assumed that if the external magnetic field is applied for seconds, the nanocomposite shows rapid aggregation within the homogenous dispersion. It is an advantageous option which means that by using an external magnet the nanocomposite can be separated from the solution, which may be beneficial in real-world applications.

The reduction in saturation magnetization in nanoparticles is due to surface effects and size effects. As nanoparticles become smaller, their surface-to-volume ratio increases, leading to a higher proportion of atoms at the surface, which may not contribute fully to the overall magnetization.

The magnetic properties of pure $CuFe_2O_4$, $CuFe_2O_4$/GO, and $CuFe_2O_4$/GO/ZnO ternary nanocomposites were explained using a vibrating sample magnetometer (VSM). The hysteresis loops in Fig. 6d show that the magnetization (Ms) of the ternary nanocomposite is lower compared to pure $CuFe_2O_4$ nanoparticles. This reduction in Ms can be attributed to the presence of GO and ZnO nanoparticles, which may disrupt the magnetic ordering of $CuFe_2O_4$ nanoparticles.

The Sawatzky model is a theoretical framework used to describe the magnetic properties of spinel ferrites. It is based on the idea that the magnetic moments of the transition metal ions (Cu^{2+} and Fe^{3+}) are aligned in a specific manner to produce the observed magnetic behavior. The model is appropriate for the sample because it takes into account the magnetic interactions between the transition metal ions and the oxygen ions in the spinel lattice. The reduction in Ms observed in the ternary nanocomposite can be explained by the Sawatzky model, which suggests that the magnetic moments of the transition metal ions are affected by the presence of GO and ZnO nanoparticles. This disruption in magnetic ordering leads to a decrease in the overall magnetization of the nanocomposite and these results are also following this model.

3.7. Electrical analysis

The electrical properties of $CuFe_2O_4$/GO/ZnO ternary nanocomposite were analyzed in order of the frequency range of 20 mHz–2 MHz and are shown in Fig. 7a, b. The electrical analysis depends on two parameters which are as follows.

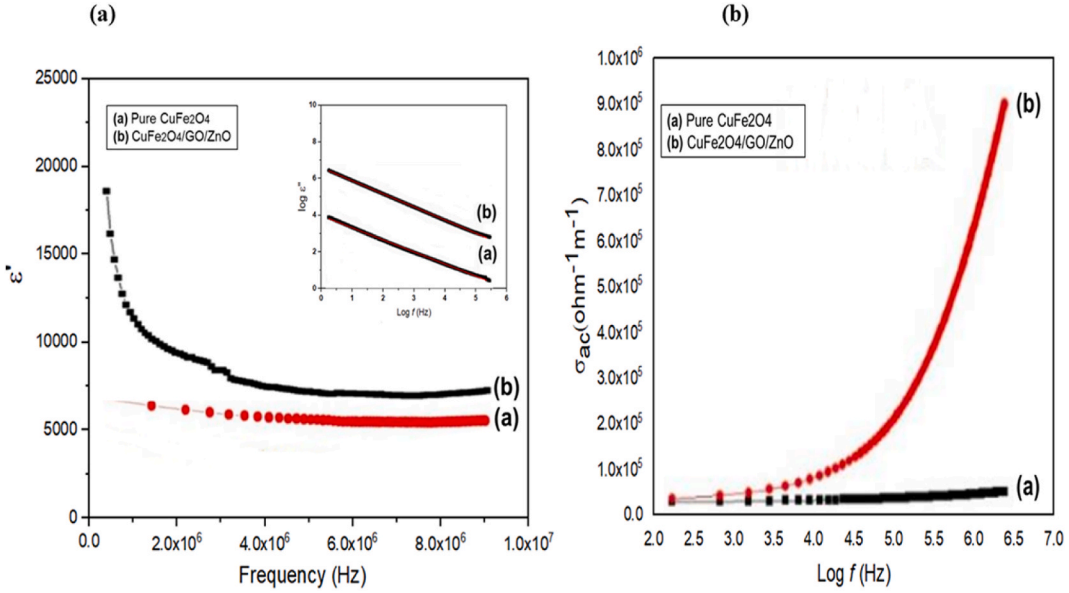

Fig. 7. Electrical properties of pure $CuFe_2O_4$ nanoparticles and $CuFe_2O_4$/GO/ZnO ternary nanocomposite are (a) real (ε') and imaginary (ε'') values of dielectric constant (b) AC conductivity.

3.7.1. Dielectric parameters

The dielectric property depends on two traits representing energy stored and energy loss within the dielectric material when an outer electric field is implemented. The dielectric can be calculated by $\varepsilon^* = \varepsilon' + i\varepsilon''$ and $\varepsilon'' = \varepsilon' \tan\delta$ where $\varepsilon'$is the real element for energy storage $\varepsilon''$is the imaginary element for energy loss and tanδ is tangent loss. Whereas the value of permittivity for free space is ($\varepsilon = 8.85*10^{-12}$ F/m) [30].

At low frequencies, the value of ε' increased while with time at higher frequencies, the value starts to degenerate and becomes too small which is also described in the literature for the spinel ferrites [31]. According to Maxwell-Wagner's theory, the large value of ε' at small frequency is due to the polarization of space charge which may cause in-homogeneity due to impurities or grain boundaries originally isolated in nature. The small frequency value could be tested by taking log (ω) at the x-axis and log (ε'') at the y-axis as shown in the inset graph of Fig. 7a. The linear line shows the accuracy of Maxwell-Wagner's theory yields at 0.987 and 0.990 for pure $CuFe_2O_4$ nanoparticles and $CuFe_2O_4$/GO/ZnO ternary nanocomposite. During the interaction of charge carriers Cu^{1+} and Fe^{2+} ions may also be the reason for the rising of dielectric polarization by the electric field produced during interaction. Same as for dielectric loss, the value of tanδ is at large when the frequency is low and starts to reduce with the enhancement in frequency reliable to ε' plot.

At lower frequencies, the dielectric constant (ε') increases, but at higher frequencies, it begins to decrease, consistent with observations in the literature for spinel ferrites [30]. Maxwell-Wagner's theory attributes the high ε' value at low frequency to space charge polarization, which may arise from impurities or grain boundaries initially isolated. To validate this behavior, a log-log plot of frequency (ω) versus ε'' can be examined, as shown in the inset graph of Fig. 7a. The linear relationship confirms the accuracy of Maxwell-Wagner's theory, yielding coefficients of determination (R^2) of 0.987 and 0.990 for pure $CuFe_2O_4$ nanoparticles and the $CuFe_2O_4$/GO/ZnO ternary nanocomposite, respectively. Additionally, the interaction between charge carriers (Cu^{1+} and Fe^{2+} ions) contributes to dielectric polarization due to the electric field generated during their interaction. Similarly, the loss tangent (tanδ) exhibits a large value at low frequencies, gradually decreasing with increasing frequency, consistent with the ε' behavior. Furthermore, this behavior is often associated with relaxation processes and the time required for dipoles or charge carriers to respond to the changing electric field.

Furthermore, adding up GO/ZnO nanoparticles within $CuFe_2O_4$ nanoparticles, the dielectric properties changed drastically. The decline in dielectric parameters with change in frequency values is due to the charge carriers smattering and production of the electric field. This is due to the space charge polarization, which occurs when the carriers accumulate. The orientation of the dipoles took more time under high frequency resulting reduction in the value of ε' and achieving the constant value [32]. In simple words, due to high frequency, the dipoles won't be able to rotate when an electric field is applied/produced thus, the dielectric constant declines. This shows that the addition of GO and ZnO content in pure $CuFe_2O_4$ nanoparticles leads to reduce the value of the dielectric constant further enhancing the electrical property of the nanocomposite.

Upon incorporating GO/ZnO nanoparticles into $CuFe_2O_4$ nanoparticles, significant changes in dielectric properties were observed. The decrease in dielectric parameters with increasing frequency can be attributed to charge carrier scattering and electric field generation. Space charge polarization occurs as carriers accumulate, affecting the orientation of dipoles. At higher frequencies, the dipoles require more time to respond, resulting in a reduction of the dielectric constant (ε') and eventual stabilization [32]. In simpler

terms, the dielectric constant declines due to hindered dipole rotation under high-frequency electric fields. Overall, the addition of GO and ZnO content to pure $CuFe_2O_4$ nanoparticles further enhances the electrical properties of the nanocomposite.

As for the variation in (ε'') concerning frequency, the value of ε'' increases at low frequencies due to the dipole polarization and decreases at high frequencies hence contributing to an improvement in the value of the dipole loss in $CuFe_2O_4$/GO/ZnO ternary nanocomposite. Moreover, Maxwell-Wagner's theory also shows the linear fit for ternary nanocomposite which yields at low values and further moves to high values. The tangent loss in $CuFe_2O_4$/GO/ZnO ternary nanocomposite increases with enhancing ZnO nanoparticles and has high dielectric loss at higher frequencies further on with the addition of GO shows a decline at high frequencies. Overall, high dielectric loss at small frequencies in $CuFe_2O_4$/GO/ZnO ternary nanocomposite is being observed which could be attributed to strong resistivity at small frequencies. The changes within the values of ε' and ε'' are due to space charge polarization. The larger values of dielectric loss at small frequencies claim that the polarization is greater of $CuFe_2O_4$/GO/ZnO ternary nanocomposite.

In the $CuFe_2O_4$/GO/ZnO ternary nanocomposite, the dielectric loss (ε'') exhibits frequency-dependent behavior. At low frequencies, ε'' increases due to dipole polarization, while at high frequencies, it decreases. This trend contributes to an enhancement in dipole loss. Maxwell-Wagner's theory confirms this behavior, showing a linear fit for the ternary nanocomposite. The tangent loss in the $CuFe_2O_4$/GO/ZnO ternary nanocomposite increases with ZnO nanoparticle content and remains high at higher frequencies. However, with the addition of GO, the tangent loss declines at high frequencies. Notably, the nanocomposite exhibits significant dielectric loss at small frequencies, likely attributed to strong resistivity. The variations in ε' and ε'' values are influenced by space charge polarization. The higher dielectric loss at small frequencies suggests greater polarization in the $CuFe_2O_4$/GO/ZnO ternary nanocomposite.

3.7.2. AC conductivity

The high conduction and resistivity phenomena of the pure $CuFe_2O_4$ and $CuFe_2O_4$/GO/ZnO ternary as-synthesized sample, the AC conductivity in the range of frequency was evaluated by equation $\sigma_{ac} = 2f\varepsilon_o\varepsilon' \tan\delta$ where C is capacitance measured in Farad (F) and ε_o is the relative permittivity for free space ($8.85 * 10^{-12}$ F/m) and f is frequency. The AC conductivity is dependent on frequency which is owing to interface charge polarization as well as intrinsic electric dipole polarization. The AC conductivity plots of pure $CuFe_2O_4$ nanoparticles are shown in Fig. 7b. As we discussed Maxwell-Wagner's equation earlier, shows the increase in conductivity as the frequency goes higher [33]. According to the above equation, the dielectric constant consists of two deposits – one is grains, and the other is grain boundaries. These layers have low and high electrical resistance points. Normally, at a low resistance point, the conductivity is low due to ideal crystalline properties. The sample becomes less conductive when the grain boundaries are set off insulated and highly active at low frequency and create a resistance that causes the electronic charge carriers to lessen their motion. At high frequencies, the involvement of grain boundary becomes negligible, and the conductivity rises due to the motion of conductive grains. As seen, this evaluation matches with the previous literature [34] in which it is suggested that the AC conductivity enhanced with the transfer of electrons between Cu^+, Cu^{2+} and Fe^{2+}, Fe^{3+} ferrite materials. When the electronic transitions (from lower to high energy level)decrease, the AC conductivity also. Low conduction of carriers happens at frequencies (10^3–10^4 Hz) whereas the mobility of electronic charges is enhanced at higher frequencies (equal to or more than 10^4 Hz) [35]. The movement of charge carriers from A site to B site, which happens to be tetra and octahedral sites, alters the semiconducting phase band into a metallic phase band. Additionally, according to XRD crystallites, the size also increases the AC conductivity phenomena.

The AC conductivity of the as-synthesized pure CuFe2O4 and $CuFe_2O_4$/GO/ZnO ternary samples was evaluated within a frequency range using the equation $\sigma_{ac} = 2f\varepsilon_o\varepsilon' \tan\delta$, ε_o is the relative permittivity for free space (8.85 × 10^-12 F/m), and f denotes frequency. The frequency-dependent behavior of AC conductivity arises from both interface charge polarization and intrinsic electric dipole polarization. In Fig. 7b, the AC conductivity plots for pure $CuFe_2O_4$ nanoparticles are presented. As previously discussed with Maxwell-Wagner's equation, conductivity increases with higher frequencies [33]. The dielectric constant comprises contributions from grain and grain boundary layers. At low resistance points (associated with ideal crystalline properties), the sample exhibits lower conductivity. Conversely, when grain boundaries become highly active at low frequencies, they create resistance, limiting electronic charge carrier mobility. At higher frequencies, grain boundary effects diminish, leading to increased conductivity due to the motion of conductive grains. This behavior aligns with previous literature suggesting enhanced AC conductivity through electron transfer between Cu^+, Cu^{2+}, Fe^{2+}, and Fe^{3+} ferrite materials [33]. Notably, low carrier conduction occurs at frequencies between 10^3 and 10^4 Hz, while electronic charge mobility improves at frequencies equal to or greater than 10^4 Hz [35]. The movement of charge carriers between A and B sites (tetrahedral and octahedral sites) transforms the semiconducting phase band into a metallic phase band. Additionally, the AC conductivity is influenced by the crystallite size, as observed from XRD data.

As far as $CuFe_2O_4$/GO/ZnO ternary nanocomposite, the addition of GO and ZnO nanoparticles influences the AC conductivity as shown in Fig. 7b.The AC conductivity of $CuFe_2O_4$/GO/ZnO ternary nanocomposite increases when the charge carriers shift between various surface localized centers as a fallout of increased frequency due to which electrons (charge carriers) hops. At low frequencies, the resistance causes the electrode interface to change the impedance of charge carriers which results in low ac conductivity of $CuFe_2O_4$/GO/ZnO ternary nanocomposite. The ZnO nanoparticles improve the ac conductivity more than the addition of GO [32]. The conductivity increases when the charge carriers migrate between spinel ferrite and semiconducting bandgap (low and high energy levels) nanomaterials when high frequency is applied.

In the $CuFe_2O_4$/GO/ZnO ternary nanocomposite, the addition of graphene oxide (GO) and zinc oxide (ZnO) nanoparticles significantly impacts AC conductivity, as depicted in Fig. 7b. As frequency increases, charge carriers transition between various surface-localized centers, resulting in electron hopping. At low frequencies, resistance alters the impedance of charge carriers at the electrode interface, leading to reduced AC conductivity in the $CuFe_2O_4$/GO/ZnO ternary nanocomposite. Interestingly, ZnO nanoparticles enhance AC conductivity more effectively than the addition of GO. Furthermore, the conductivity increases as charge carriers

migrate between spinel ferrite and semiconducting bandgap nanomaterials, corresponding to low and high energy levels, respectively, under the influence of high-frequency fields.

The ternary nanocomposite possesses high resistance and capacitance at lower frequencies. The resistance increased with the addition of GO and ZnO content but was lower with the increase in the frequency values reaching up to 2 MHz. Whereas the capacitance rises for $CuFe_2O_4$/GO/ZnO ternary nanocomposite as compared to pure $CuFe_2O_4$ nanoparticles [32].

At lower frequencies, the $CuFe_2O_4$/GO/ZnO ternary nanocomposite exhibits elevated resistance and capacitance. The resistance increases with the addition of graphene oxide (GO) and zinc oxide (ZnO) content, but as the frequency surpasses 2 MHz, the resistance decreases. In contrast, the capacitance of the $CuFe_2O_4$/GO/ZnO ternary nanocomposite surpasses that of pure $CuFe_2O_4$ nanoparticles [32]. While summarizing, the dielectric constant (ε') and tangent loss (tanδ) were evaluated across a frequency range up to 2 MHz. Notably, ε' and tanδ exhibit a decline at higher frequencies, signifying reduced energy storage and energy loss within the dielectric material. This behavior aligns with the expected characteristics of dielectric materials, where the dielectric constant tends to decrease at higher frequencies due to diminished energy storage capacity. Additionally, the AC conductivity was measured within the same frequency range. Interestingly, the AC conductivity increases at lower frequencies, indicating enhanced electrical conductivity. This trend is consistent with the anticipated behavior of AC conductivity, where conductivity typically rises at lower frequencies due to improved charge carrier mobility.

4. Conclusions

Copper ferrite/Graphene Oxide and Zinc Oxide ($CuFe_2O_4$/GO/ZnO) ternary nanocomposite have been synthesized by hydrothermal process. The experimental data revealed the face-centered cubic structure of pure spinal ferrite ($CuFe_2O_4$) nanoparticles. The peak observed at $2\theta(31.70^\circ)$ with an hkl value (220) indicates the successful addition of ZnO in $CuFe_2O_4$/GO nanocomposite. In the XRD graph, the absence of the characteristic peak of GO revealed the intercalation of $CuFe_2O_4$ nanoparticles with graphene oxide layers. Visible light absorbance of $CuFe_2O_4$ nanoparticles increased by adding GO and ZnO content in pure $CuFe_2O_4$. By introducing GO and ZnO content in CuFe2O4 nanoparticles, the energy band gap reduces from 2.63 to 2.46 eV as compared to pure $CuFe_2O_4$ nanoparticles. In SEM analysis, agglomeration among $CuFe_2O_4$ nanoparticles with GO and ZnO has been observed due to magnetic interaction between sample nano-crystallites and high surface-to-volume ratio. The magnetic properties of as-synthesized samples have been accomplished via VSM at room temperature under 0–0.5 and ± 5 T. In the ternary nanocomposite of $CuFe_2O_4$/GO/ZnO, the value of saturation magnetization (M_s) decreases from 2.071 to 1.365 emu/g due to the addition of ZnO content. In $CuFe_2O_4$/GO/ZnOternary nanocomposite, the loops were narrowed showing a decrease in the coercive field with the addition of ZnO content in $CuFe_2O_4$/GO nanocomposite material. Moreover, the study of electrical properties of pure $CuFe_2O_4$ and $CuFe_2O_4$/GO/ZnO ternary nanocomposite revealed that the values of dielectric constant and tangent loss decrease at high frequencies owing to surface charge polarization and intrinsic dipole interactions and have high values at low frequencies and become constant at values more than 2 MHz whereas the AC conductivity of both samples was high at low frequencies while having high capacitance and resistance values.

Data availability statement

The authors confirm that the data supporting the findings of this study are available within the article. Ideas, materials, lab, and lab equipment are all done in the Physics lab of the National Textile University (NTU), Characterizations like UV, and FTIR are also done at NTU-Faisalabad, and others are done in another University in Pakistan.

If the manuscript is accepted, then this manuscript is available to the readers according to the policy of the journal. We (authors) do not have any objection.

CRediT authorship contribution statement

Saddam Hussain: Writing – Original draft, Investigation, Formal analysis, Data curation. **Samavia Rafiq:** Writing – Original draft, Investigation, Data curation, Conceptualization. **M.I. Yousaf:** Writing – original draft, Supervision, Project administration, Methodology, Investigation, Formal analysis, Data curation, Conceptualization. **Sofia Nosheen:** Writing – review & editing. **Dalal Nasser Binjawhar:** Resources, Funding acquisition, Writing – review & editing, Formal Analysis. **Mohamed M. Abdel-Daim:** Resources, Funding acquisition, Writing – review & editing, Formal Analysis.

Declaration of competing interest

All authors of this manuscript titled "**Tuning optical, magnetic, and electrical parameters of $CuFe_2O_4$ nanoparticles incorporated with GO and ZnO by using a facile synthesis**" certify that they have no affiliations with or involvement in any organization or entity with any financial interest (such as honoraria; educational grants; participation in speakers' bureaus; membership, employment, consultancies, stock ownership, or other equity interest; and expert testimony or patent-licensing arrangements), or non-financial interest (such as personal or professional relationships, affiliations, knowledge or beliefs) in the subject matter or materials discussed in this manuscript.

Acknowledgment

This study was supported by Princess Nourah bint Abdulrahman University Researchers Supporting Project number (PNURSP2024R155), Princess Nourah bint Abdulrahman University, Riyadh, Saudi Arabia.

References

[1] A. Adewuyi, R.A. Oderinde, Tartaric acid-modified CuFe2O4: potential application in the purification of butylated hydroxyanisole and butylated hydroxytoluene-contaminated water, J. Mater. Res. (2022), https://doi.org/10.1557/s43578-022-00709-9.
[2] T.M. Hammad, J.K. Salem, A.A. Amsha, N.K. Hejazy, Optical and magnetic characterizations of zinc substituted copper ferrite synthesized by a co-precipitation chemical method, J. Alloys Compd. 741 (2018 April) 123–130.
[3] U. Naresh, J. Kumar, K.C.B. Naidu, Hydrothermal synthesis of barium copper ferrite nanoparticles: nanofiber formation, optical and magnetic properties, Mater. Chem. Phys. 236 (2019 Oct) 121807.
[4] N.A. Singh, Nanotechnology innovations, industrial applications, and patents, Environ. Chem. Lett. 15 (2) (2017 Jun) 185–191.
[5] C.A. Charitidis, P. Georgiou, M.A. Koklioti, A.F. Trompeta, V. Markakis, Manufacturing nanomaterials: from research to industry, Manuf. Rev. 1 (2014) 11.
[6] K.A. Hamzah, C.K. Yeoh, M.M. Noor, P.L. Teh, Y.Y. Aw, S.A. Sazali, W.M. Wan Ibrahim, Mechanical properties and thermal and electrical conductivity of 3D printed ABS-copper ferrite composites via 3D printing technique, J. Thermoplast. Compos. Mater. 35 (1) (2022 Jan) 3–16.
[7] M.A. Camacho-Gonzalez, M. Quezada-Cruz, G.I. Ceron-Montes, M.F. Ramirez-Ayala, L.E. Hernandez-Criz, A. Garrido-Hernandez, Synthesis and characterization of magnetic zinc-copper ferrites: antibacterial activity, photodegradation study, and heavy metals removal evaluation, Mater. Chem. Phys. 236 (2019 Oct) 121808.
[8] M. Sajjad, I. Ullah, M.I. Khan, J. Khan, M.Y. Khan, M.T. Qureshi, Structural and optical properties of pure and copper-doped zinc oxide nanoparticles, Results Phys. 9 (2018 Jun) 1301–1309.
[9] J. Huang, Z. Yin, Q. Zheng, Applications of ZnO in organic and hybrid solar cells, Energy Environ. Sci. 4 (10) (2011) 3861–3877.
[10] M.T. Noman, N. Amor, M. Petru, Synthesis and applications of ZnO nanostructures (ZONSs): a review, Crit. Rev. Solid State Mater. Sci. 47 (2) (2022 Mar 4) 99–141.
[11] M. Shekofteh-Gohari, A. Habibi-Yangjeh, M. Abitorabi, A. Rouhi, Magnetically separable nanocomposites based on ZnO and their applications in photocatalytic processes: a review, Crit. Rev. Environ. Sci. Technol. 48 (10–12) (2018 Jun 18) 806–857.
[12] R. You, Y.Q. Liu, Y.L. Hao, D.D. Han, Y.L. Zhang, Z. You, Laser fabrication of graphene-based flexible electronics, Adv. Mater. 32 (15) (2020 Apr) 1901981.
[13] L. Kumaresan, M. Mahalakshmi, M. Palanichamy, V. Murugesan, Synthesis, characterization, and photocatalytic activity of Sr2+ doped TiO_2 nanoplates, Ind. Eng. Chem. Res. 49 (2010) 1480–1485.
[14] G.H. Le, Q.T. Ngo, Q.K. Nyugen, T.T. Quan, T.A. Vu, Highly photocatalytic activity of novel $CuFe_2O_4$/GO nanocomposite in the degradation of phenol from aqueous solution, Phys. Chem. 7 (1) (2017) 8–16.
[15] L. Nirumand, S. Farhadi, A. Zabardasti, A. Khataee, Copper ferrite nanoparticles supported on MIL-101/reduced graphene oxide as an efficient and recyclable sonocatalyst, J. Taiwan Inst. Chem. Eng. 93 (2018 Dec) 674–685.
[16] Z. Shahnavaz, P.M. Woi, Y. Alias, A hydrothermally prepared reduced graphene oxide-supported copper ferrite hybrid for glucose sensing, Ceram. Int. 41 (10) (2015 Dec) 12710–12716.
[17] A. Kumar, L. Rout, L.S. Achary, R. Dhaka, P. Dash, Greener route for synthesis of aryl and alkyl-14H-dibenzo [a.j.] xanthenes using graphene oxide-copper ferrite nanocomposite as a recyclable heterogeneous catalyst, Sci. Rep. 7 (1) (2017 Feb) 1–8.
[18] P. Yadav, P.K. Surolia, D. Vaya, Synthesis and application of copper ferrite-graphene oxide nanocomposite photocatalyst for the degradation of malachite green, Mater. Today: Proc. 43 (2021 Jan 1) 2949–2953.
[19] R. Kodasma, B. Palas, G. Ersöz, S. Atalay, Photocatalytic activity of copper ferrite graphene oxide particles for an efficient catalytic degradation of Reactive Black 5 in water, Ceram. Int. 46 (5) (2020 Apr 1) 6284–6292.
[20] A. Kumar, L. Rout, L.S.K. Achary, S.K. Mohanty, P. Dash, A combustion synthesis route for magnetically separable graphene oxide-CuFe2O4-ZnO nanocomposites with enhanced solar light-mediated photocatalytic activity, New J. Chem. 41 (19) (2017) 10568–10583, https://doi.org/10.1039/c7nj02070h.
[21] M. Khairy, W.A. Bayoumy, S.S. Selima, M.A. Mousa, Studies on characterization, magnetic and electrochemical properties of nano-size pure and mixed ternary transition metal ferrites prepared by the auto-combustion method, J. Mater. Res. 35 (20) (2020 Oct) 2652–2663.
[22] L. Khanna, G. Gupta, S.K. Tripathi, Effect of size and silica coating on structural, magnetic as well as cytotoxicity properties of copper ferrite nanoparticles, Mater. Sci. Eng. C 97 (2019 Apr) 552–566.
[23] M. Sajjad, I. Ullah, M.I. Khan, J. Khan, M.Y. Khan, M.T. Qureshi, Structural and optical properties of pure and copper doped zinc oxide nanoparticles, Results Phys. 9 (2018 Jun) 1301–1309.
[24] A. Zourou, A. Ntziouni, N. Adamopoulos, T. Roman, F. Zhang, M. Terrones, K. Kordatos, Graphene oxide-CuFe2O4 nanohybrid material as an adsorbent of Congo red dye, Carbon Trends 7 (2022 Apr) 100147.
[25] S. Singh, A. Sahai, S.C. Katyal, N. Goswami, Structural, optical and vibrational study of zinc copper ferrite nanocomposite prepared by exploding wire technique, Mater. Sci. Pol 36 (2018) 722–732.
[26] S.P. Keerthana, R. Yuvakkumar, G. Ravi, S. Pavithra, M. Thambidurai, C. Dang, D. Velauthapillai, Pure and Ce-doped spinel CuFe2O4 photocatalysts for efficient rhodamine B degradation, Environ. Res. (2021) 111528.
[27] T.M. Hammad, J.K. Salem, A.A. Amsha, N.K. Hejazy, Optical and magnetic characterizations of zinc substituted copper ferrite synthesized by a co-precipitation chemical method, J. Alloys Compd. 741 (2018) 123–130.
[28] V. Jeseentharani, M. George, B. Jeyaraj, A. Dayalan, K.S. Nagaraja, Synthesis of metal ferrite (MFe2O4, M= Co, Cu, Mg, Ni, Zn) nanoparticles as humidity sensor materials, J. Exp. Nanosci. 8 (3) (2013) 358–370.
[29] N. Masunga, O.K. Mmelesi, K.K. Kefeni, B.B. Mamba, Recent advances in copper ferrite nanoparticles and nanocomposites synthesis, magnetic properties and application in water treatment, J. Environ. Chem. Eng. 7 (3) (2019 Jun) 103179.
[30] E.R. Kumar, R. Jayaprakash, G.S. Devi, P.S. Reddy, Magnetic, dielectric, and sensing properties of manganese substituted copper ferrite nanoparticles, J. Magn. Magn Mater. 355 (2014 Apr) 87–92.
[31] G. Channagoudra, A.K. Saw, V. Dayal, Role of structure and cation distribution on magnetic and electrical properties in inverse spinel copper ferrite, J. Phys. Chem. Solid. 154 (2021 Jul) 110086.
[32] V. Mututu, A.K. Sunitha, R. Thomas, M. Pandey, B. Manoj, An investigation on structural, electrical, and optical properties of GO/ZnO nanocomposite, Int. J. Electrochem. Sci. 14 (3752–3763) (2019 Apr 1) 3752.
[33] K. Verma, A. Kumar, D. Varshney, Effect of Zn and Mg doping on structural, dielectric, and magnetic properties of tetragonal CuFe2O4, Curr. Appl. Phys. 13 (3) (2013 May) 467–473.
[34] A.M. Farea, S. Kumar, K.M. Batoo, A. Yousef, C.G. Lee, Influence of the doping of Ti4+ ions on electrical and magnetic properties of Mn1+ xFe2− 2xTixO4 ferrite, J. Alloys Compd. 469 (1–2) (2009 Feb) 451–457.
[35] F.H. Mulud, N.A. Dahham, I.F. Waheed, Synthesis and characterization of copper ferrite nanoparticles, IOP Conf. Ser. Mater. Sci. Eng. 928 (2020) 072125.